

Rapid #: -22551902

CROSS REF ID: **35204970830001852**

LENDER: **CFI (California State Univ., Fullerton) :: Pollak Library**

BORROWER: **ORU (University of Oregon) :: Main Library**

TYPE: Article CC:CCG

JOURNAL TITLE: Engineering geology

USER JOURNAL TITLE: Engineering geology

ARTICLE TITLE: Predicting the sliding behavior of rotational landslides based on the tilting measurement of the slope surface

ARTICLE AUTHOR: Xie, Jiren ; Uchimura, Taro ; Wang, Gonghui ; Selv

VOLUME: 269

ISSUE:

MONTH:

YEAR: 2020

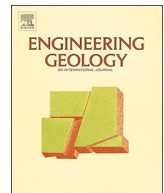
PAGES: 105554

ISSN: 0013-7952

OCLC #: 38907779

Processed by RapidX: 5/8/2024 5:14:43 PM

This material may be protected by copyright law (Title 17 U.S. Code)



Predicting the sliding behavior of rotational landslides based on the tilting measurement of the slope surface

Jiren Xie^{a,b,*}, Taro Uchimura^c, Gonghui Wang^d, Hemakanth Selvarajah^e, Zain Maqsood^b, Quan Shen^{f,g}, Guoxiong Mei^f, Shifan Qiao^{a,*}

^a Department of Civil Engineering, Central South University, Changsha, Hunan 410075, China

^b Department of Civil Engineering, The University of Tokyo, 7-3-1, Hongo, Bunkyo-ku, Tokyo, 113-8656, Japan

^c Department of Civil and Environmental Engineering, Saitama University, 255 Shimo-Okubo, Sakura-ku, Saitama 338-8570, Japan

^d Disaster Prevention Research Institute, Kyoto University, Uji, Kyoto 611-0011, Japan

^e National Graduate Institute for Policy Studies, Roppongi, Minato-ku, Tokyo 106-8677, Japan

^f College of Civil Engineering and Architecture, GuangXi University, Nanning 530004, China

^g Department of Civil Engineering, Hunan University of Technology, Zhuzhou, Hunan 412000, China



ARTICLE INFO

Keywords:

Slope surface tilting
Surface tilting measurement
Surface displacements
Slip surface
Rotational landslides

ABSTRACT

The surface displacements of slopes have been considered as a significant indicator in landslide investigations in last several decades, while in recent years the tilting of slope surfaces is also being recognized as an important index in landslide monitoring. However, the slope surface tilting has been rarely examined so far, and requires detailed investigations. In this paper, a series of laboratory tests and a field test were performed to investigate the surface tilting in rotational landslides, as well as the correlation between tilt angles and displacements of slope surfaces. In the laboratory tests, slope models were constructed with different shapes of pre-designed slip surfaces, and tested under varying test conditions. The tilting behavior of the slope surfaces in laboratory tests was measured using tilt sensors embedded into the slopes, while the surface displacement was obtained by tracing the movement of marked points set on the slope surfaces near to the tilt sensors. The test results revealed a linear relationship between the tilt angles and displacements of slope surfaces in the process of slope failure, and this linear relationship was validated by a field test in which the slope failure was triggered by artificial rainfall. The test results also indicated that the coefficient of the linear relation is consistent with the value of real distance between the locations of tilt sensors and the centers of slip surfaces. An equation that relates the slope surface tilting and displacements was proposed in this study. Furthermore, a method to estimate the geometry of the slip surface was also developed, which was deduced from the observation that the path of the sliding masses was parallel to the slip surface according to the results of laboratory tests. Additionally, an acceleration stage of surface tilting was observed in slope failure induced by artificial rainfall, which implies that the surface tilting measurement can be used to predict the potential development of a rotational landslide or its reactivation.

1. Introduction

In recent years, the losses of properties as well as human lives caused by landslide disasters have shown an increasing trend, and this has led to investigations on landslide disaster mitigation and the early warning techniques of landslides (Stähli et al., 2015; Uhlemann et al., 2016; Dixon et al., 2018). The typical techniques for landslide disaster mitigation, such as retaining walls and ground anchors, are costly and not suitable for a large number of slopes. In this context, the early warning systems for landslides are promising methods to estimate the risks of landslides and mitigate the damage caused by landslides (Teuku

et al., 2016; Smethurst et al., 2017).

In last several decades, the displacements of slope surfaces have been considered as a significant indicator for landslide prediction (Kuroki et al., 1995; Ochiai et al., 2004; Iverson et al., 2000; Wang and Sassa, 2003; Intrieri et al., 2012). Some prediction methods for the occurrence of landslides based on the time history of the surface displacement of slopes were proposed, which were deduced from the creep theories and validated by many research groups (Saito, 1969; Fukuzono, 1985; Voight, 1988; Petley et al., 2002; Crosta and Agliardi, 2003; Sornette et al., 2004; Intrieri et al., 2017). Although a variety of conventional techniques for surface displacement measurements using

* Corresponding authors at: Department of Civil Engineering, Central South University, Changsha, Hunan 410075, China.

E-mail address: qiaoshifan@163.com (S. Qiao).

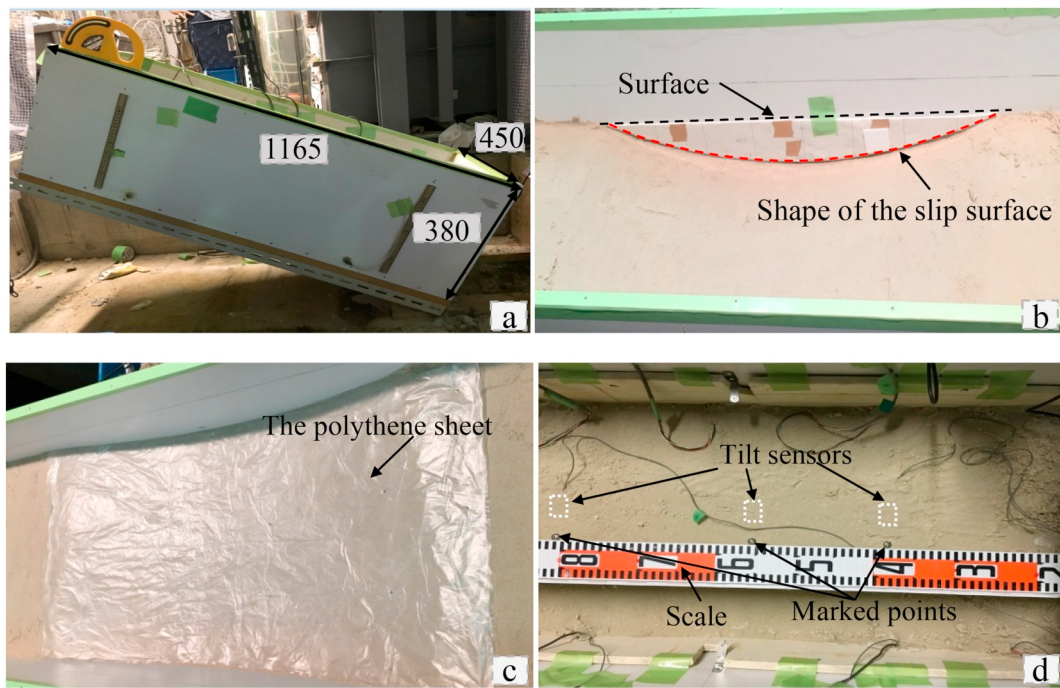


Fig. 1. Images of the laboratory test steps. (a) The dimensions of the container, (b) Make the slip surface, (c) Set the polythene sheet, (d) Build the surface layer and install instruments.

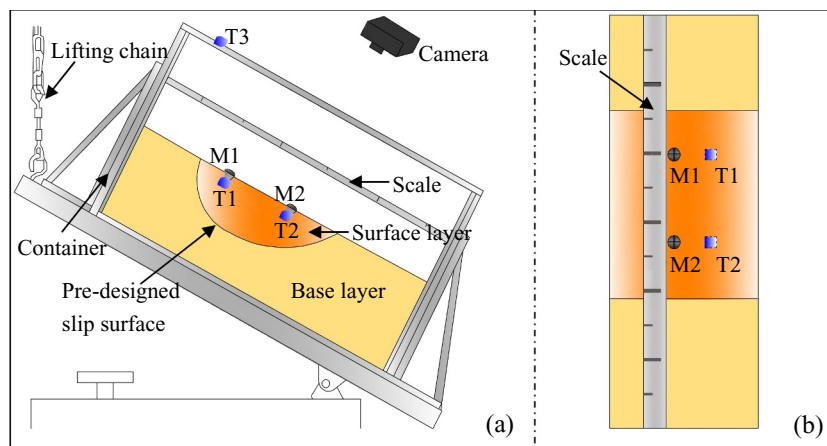


Fig. 2. Schematic illustration of the model tests. (a) The cross section of the slope model, (b) The experimental setup in the test. T1, T2 and T3 are tilt sensors, while M1 and M2 are the marked points set at the vicinity of the tilt sensors.

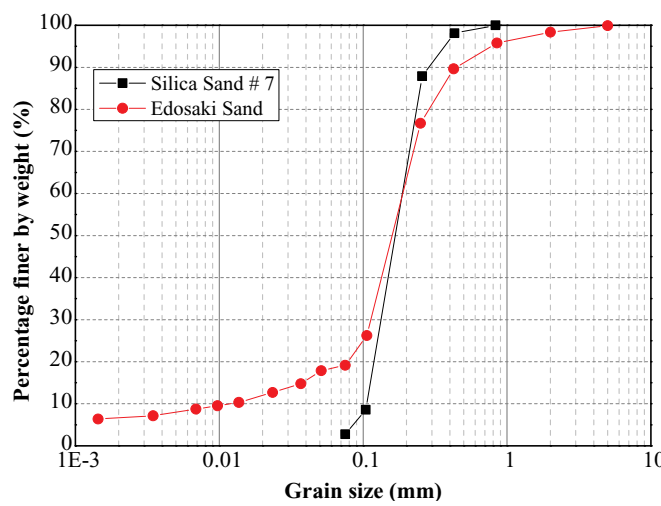


Fig. 3. Particle size distribution of Silica Sand number 7 and Edosaki Sand.

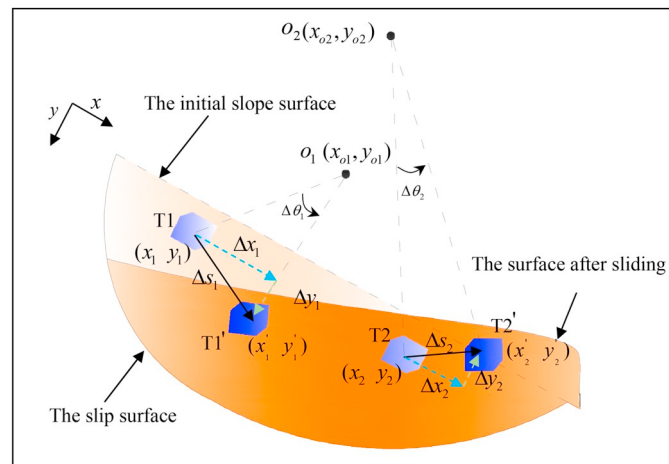


Fig. 4. The illustration of slope deformation.

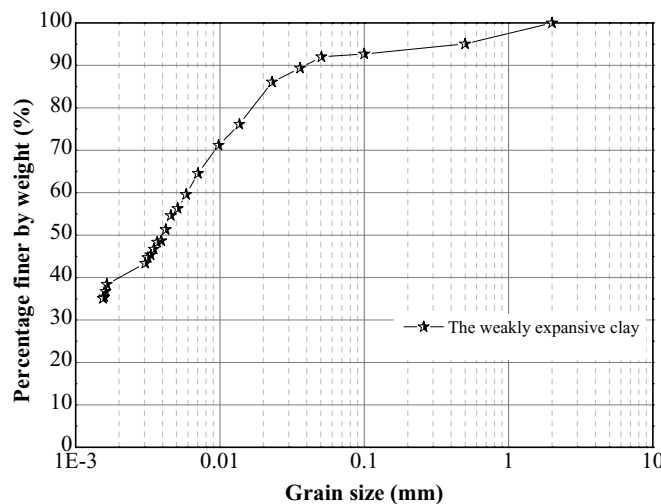


Fig. 5. Particle size distribution of the material in the field test (after Xie et al., 2019).

crackmeters or extensometers have been employed in landslide monitoring (Intriери et al., 2012; Smethurst et al., 2017; Carlà et al., 2018), the complexity in instrument installation and high costs for the

associated maintenance limit the application of these techniques (Uchimura et al., 2015). With the development of remote sensing methods, InSAR technology and terrestrial laser scanning techniques have been employed in slope monitoring for surface displacement observation (e.g. Jaboyedoff et al., 2009; Wasowski and Bovenga, 2014; Wasowski and Bovenga, 2015; Wasowski and Pisano, 2019). Usefulness of these techniques for slope surface survey is recognized, and it is also indicated that the ground investigations are typically needed to reconstruct the sliding mechanisms of rotational landslides (Jaboyedoff et al., 2009; Wasowski and Pisano, 2019).

As regards in situ investigations, slope tilting monitoring systems were also developed to measure the pre-failure surface tilting behavior of slopes in recent years (Towhata et al., 2005; Uchimura et al., 2010; Abhirup et al., 2018; Xie et al., 2019). In these systems, tilt sensors were attached to the steel rods and vertically installed to a depth of 1 m in the unstable slope layer. The abnormal tilting behavior of the steel rods caused by slope sliding was observed before the onset of slope failure (Uchimura et al., 2015). However, these tilting monitoring systems are only available to forewarn the pre-failure tilting behavior of shallow landslides. Additionally, it is also noteworthy that the real slope surface tilting is different from the tilting of steel rods inserted into slopes.

In this paper, investigations on the tilting behavior and movement of the slope surface were carried out by performing a series of laboratory model tests and a field test on a natural slope. In the laboratory tests, slope models with different shapes of pre-designed circular and

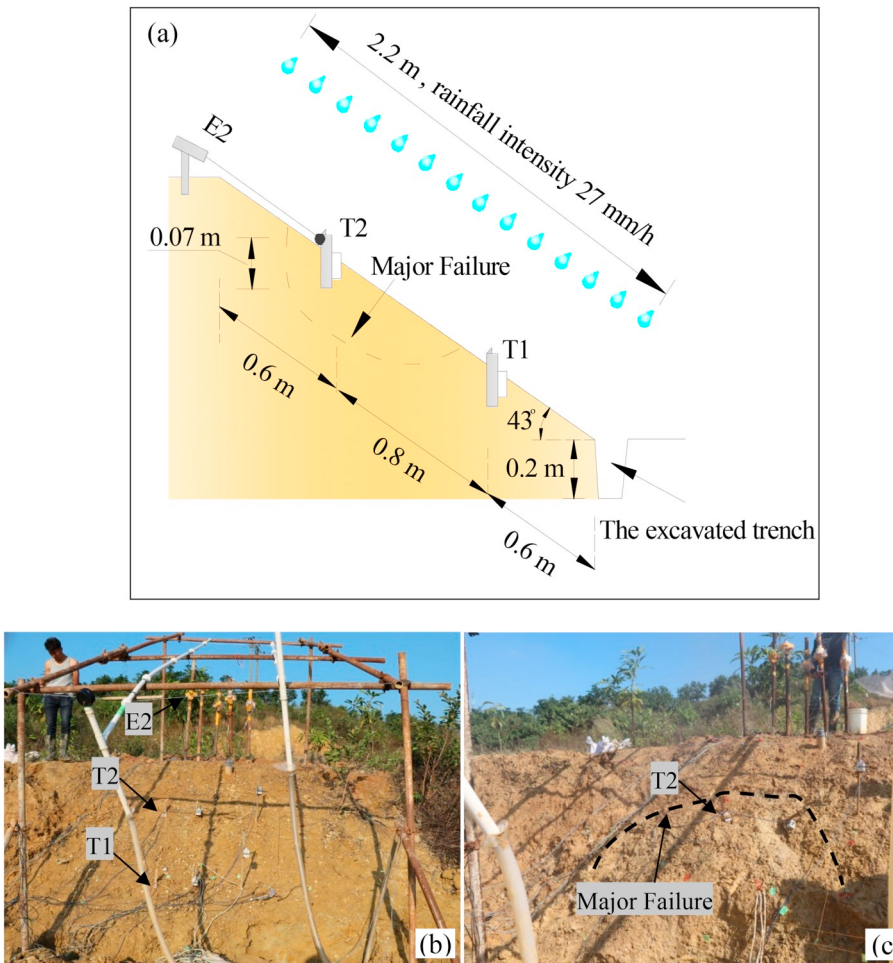


Fig. 6. The test slope in field test: (a) the cross section of the slope and experimental setup in field test, (b) The image of the slope before slope failure, (c) The image of the slope after slope failure.

Table 1

Details about the model tests.

Test No.	Materials	Radius of the slip surface(mm)	Dry density of the base layer (g/cm ³)	Dry density of the surface layer (g/cm ³)	Triggering factor
1	Silica sand #7	R1000	1.60	1.32	Tilting the container
2	Edosaki sand	R600	1.70	1.25	Tilting the container
3	Edosaki sand	R600 + R400	1.70	1.25	Tilting the container
4	Silica sand #7	R600 + R400	1.60	1.32	Tilting the container
5	Silica sand #7	R300 + R800	1.60	1.32	Tilting the container
6	Silica sand #7	R300 + R800	1.60	1.32	Periodical Rainfall
7	Silica sand #7	R300 + R800	1.60	1.32	Continuous Rainfall

noncircular slip surfaces were tested under varying conditions, such as using different materials or applying different triggering factors to induce the slope failure.

The surface tilting in the laboratory tests was measured by tilt sensors embedded into the slopes, while the displacements of the slope surfaces were obtained by tracing the movement of marked points set in the vicinity of tilt sensors. Additionally, a field test was performed on a natural slope which consisted of weakly expansive clay, and the slope failure in the field test was triggered by artificial rainfall. The tilt angles and displacements of the slope surface in this test were recorded by tilt sensors and extensometers. This study presents results of a detailed

investigation on the sliding behavior of rotational landslides, and also provides an important reference to estimate the potential development of a rotational landslide or its reactivation based on surface tilting measurements.

2. Methodology and materials

2.1. Laboratory model tests

Laboratory model tests were conducted on small-sized slope models with different pre-designed slip surfaces, and used to reconstruct the

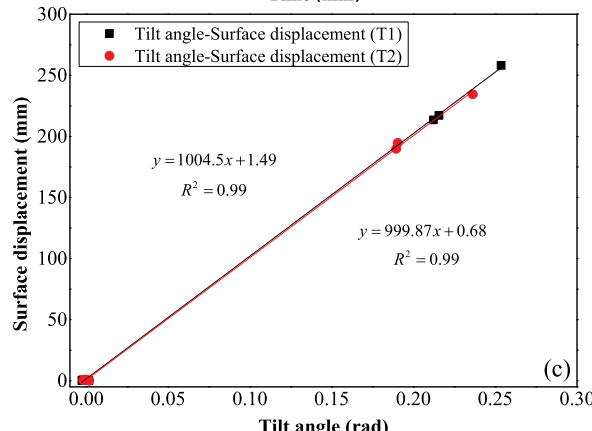
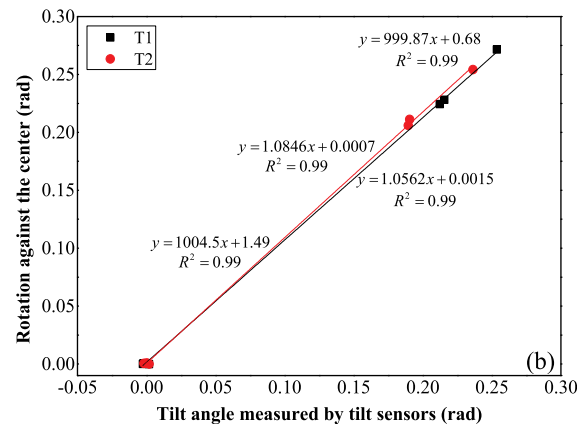
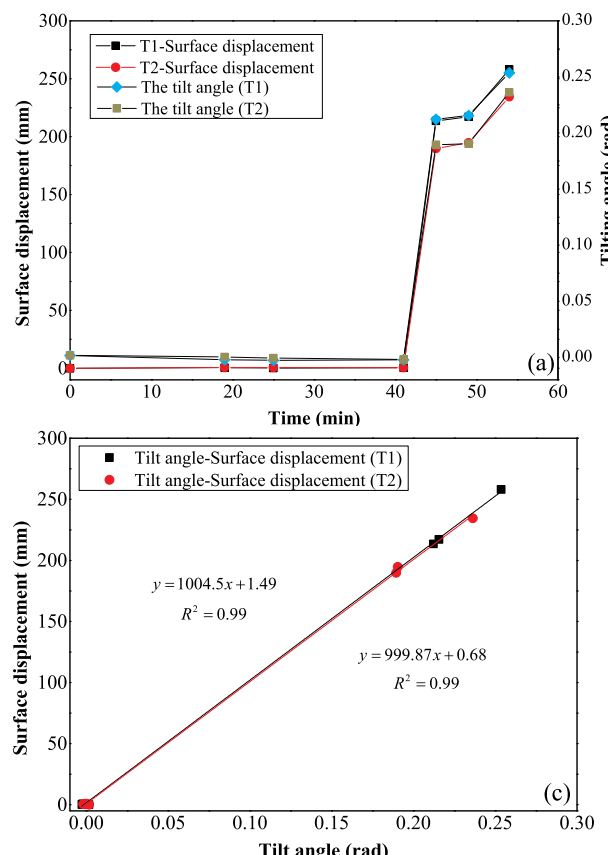


Fig. 7. Results of Test 1. (a) The surface displacements and tilt angles of the slope surface against time, (b) Relationship between the tilt angles of the slope model measured by tilt sensors and the rotational angles of the slope against the centers of the slip surface, (c) Relationship between the surface displacements and tilt angles of the slope surface.

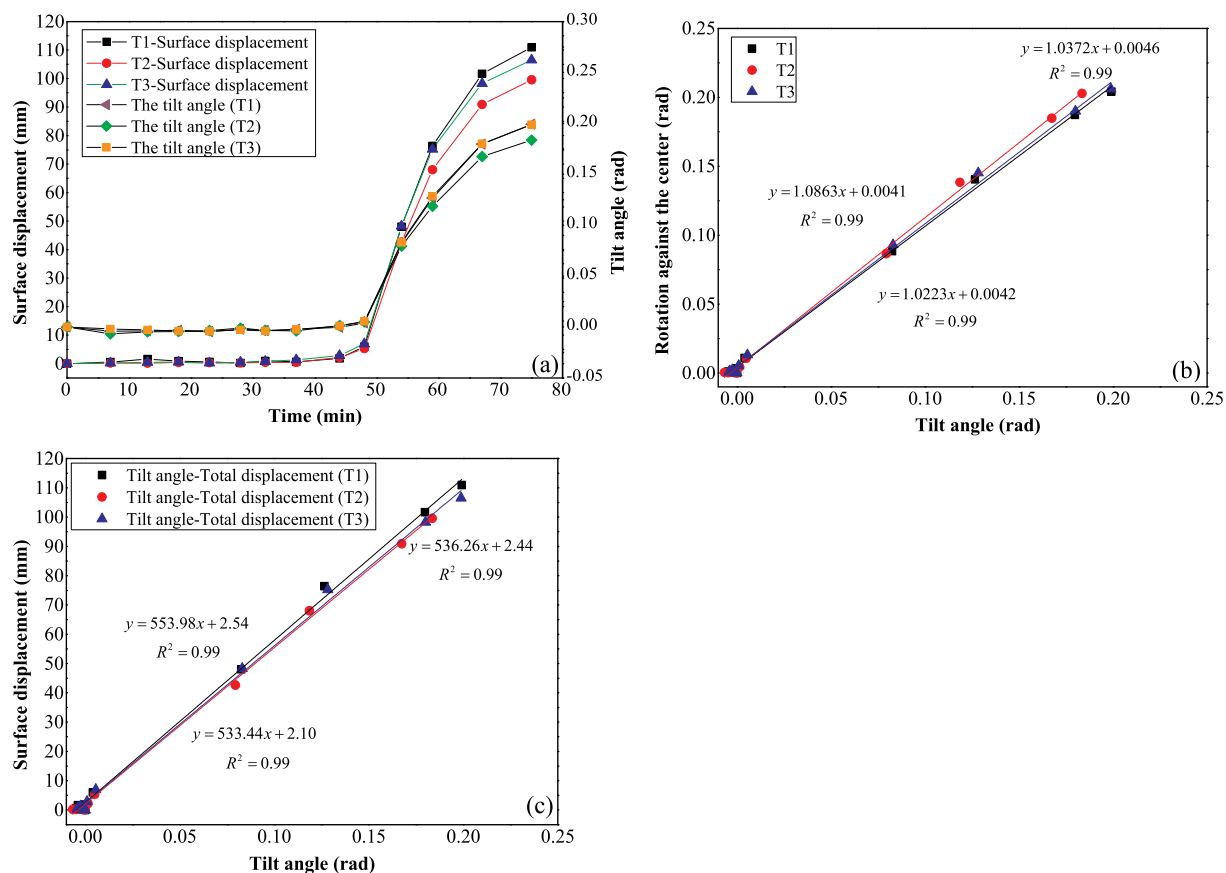


Fig. 8. Results of Test 2. (a) The surface displacements and tilt angles of the slope surface against time, (b) Relationship between the tilt angles of the slope model measured by tilt sensors and the rotational angles of the slope against the centers of the slip surface, (c) Relationship between the surface displacements and tilt angles of the slope surface.

surface sliding behavior of a rotational landslide with a weak layer or its reactivation.

The slope models were constructed in a rectangular container with the dimensions of 1165 mm (Length) \times 450 mm (Width) \times 380 mm (Height), which comprised of two layers. A pre-designed slip surface was set between these two layers using a polythene sheet to reduce the friction and restrict the water flow. Images for the procedure of slope construction are presented in Fig. 1. The schematic illustration of the slope profile and the experimental setup are shown in Fig. 2.

Materials employed in the laboratory tests are indicated in Fig. 3. As shown in Fig. 3, two kinds of soils including Silica Sand number 7 and Edosaki Sand were used in the tests. Silica Sand number 7 is a kind of commercial sands and widely used in laboratory tests, while Edosaki Sand is granular soil with a high percentage of finer content sampled from a natural slope in Ibaraki Prefecture of Japan.

For the construction of the base layer, the material was prepared at a gravimetric water content of 10% and gently compacted to the maximum dry density of the soils (1.60 g/cm³ for Silica Sand number 7 and 1.70 g/cm³ for Edosaki Sand). Subsequently, the base layer was modeled into a pre-designed shape as shown in Fig. 1(b) before building up the surface layer with a relatively looser dry density (1.32 g/cm³ for Silica Sand number 7 and 1.25 g/cm³ for Edosaki Sand). A polythene sheet was placed between the base layer and surface layer acting as the pre-designed slip surface of slopes considering that the polythene can

reduce friction and restrict water flow. Tilt sensors (T1 and T2) were embedded in slopes within a depth of 3 cm, which were utilized to measure the tilting behavior of slope surfaces. An extra tilt sensor (T3) fixed on the rectangular container was employed to record the inclination of the container as shown in Fig. 2. Additionally, marked points (M1 and M2) using nails with a length of 3 cm were set at the slope surface in the vicinity of the tilt sensors. A digital camera parallel to the slope surface was used to record the surface movement of the marked points on the slopes, and a scale installed above the slope was utilized as a reference coordinate for image analysis. The surface displacements as shown in Fig. 4 could be obtained based on the following equation.

$$\Delta s_i = \sqrt{\Delta x_i^2 + \Delta y_i^2} \quad (1)$$

where Δs_i is the surface displacements of slopes. Δx_i is the displacements parallel to the slope surface obtained based on image analysis, and Δy_i is the normal displacement measured by a vernier caliper.

Two types of model tests were conducted to investigate the surface tilting behavior, and varying triggering factors were applied in these tests to induce the slope failure. In one type of model tests, the slope failure was triggered by tilting the container gradually. The slope models in these tests were constructed with no inclination, and then tilted gradually using a lifting chain as shown in Fig. 2(a) to induce the

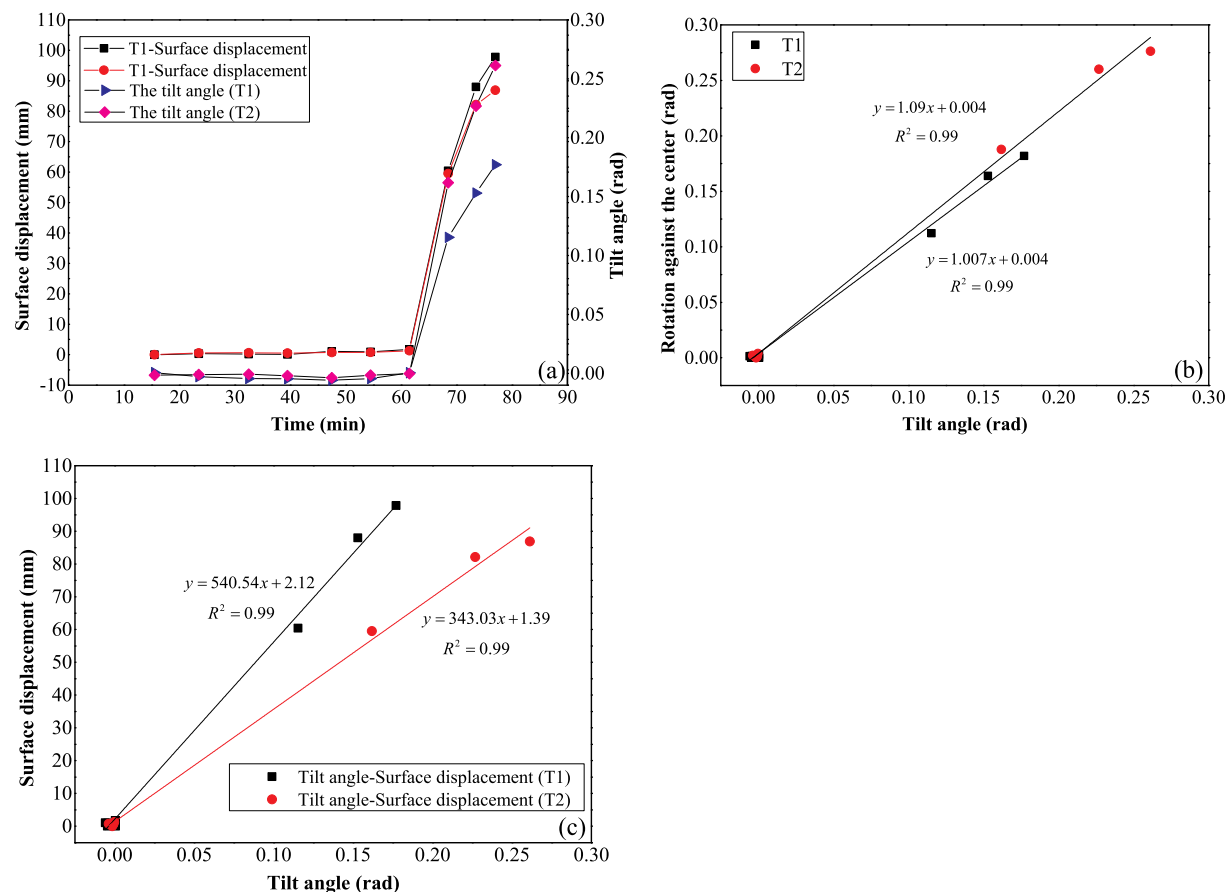


Fig. 9. Results of Test 3. (a) The surface displacements and tilt angles of the slope surface against time, (b) Relationship between the tilt angles of the slope model measured by tilt sensors and the rotational angles of the slope against the centers of the slip surface, (c) Relationship between the surface displacements and tilt angles of the slope surface.

slope failure. The triggering factor of slope failure in the other type of model tests was applying artificial rainfall. The slope models in these tests were also constructed horizontally, and rotated to a specific angle of 41.5 degree before the artificial rainfall applied.

2.2. Field test

A field test was carried out on a natural slope located in Baise city of Guangxi Province, China. The test slope consisted of weakly expansive clay, and the particle size distribution of this soil is presented in Fig. 5. The permeability of the slope layer was less than 10^{-5} cm/s based on the falling head permeability tests. However, the in situ permeability of the slope was relatively higher than the estimated value from permeability tests considering the existence of cracks at the slope surface. The slope angle was 43 degree, and the dimensions of the test slope was 2.2 m in width and 2.0 m in length along the slope direction. In this field test, two tilt sensors with short rods (T1 and T2) were employed to measure the surface tilting of the slope, and an extensometer (E2) attached to T2 was used to record the surface displacements. The slope profile and the setup of apparatus are indicated in Fig. 6. As shown in Fig. 6, a trench was excavated at the toe of the slope with a depth of 0.2 m to reduce the slope stability. After the preparation, artificial rainfall with a constant rainfall intensity of 27 mm/h was applied using

an artificial rainfall supply system, which was comprised of a pump, a water tank, two pressure gauges, eight spray nozzles and several pipelines.

3. Results

3.1. Results of laboratory model tests

Varying test conditions were applied in model tests, which are presented in Table 1. The slope profiles and the experimental setup in these tests are shown in Appendix Fig. A.

3.1.1. Results of test 1

In this test, Silica Sand number 7 was used. The dry density for the surface layer was 1.32 g/cm^3 , and it was 1.60 g/cm^3 for the base layer as shown in Table 1. A pre-designed circular slip surface with the radius of 1000 mm was set between the surface layer and base layer. The slope cross section and details of the experimental setup are illustrated in Fig. A(a). The slope failure in this test was induced by increasing the inclination of the slope gradually. With the increase of the inclination, the slope became unstable and finally slid along the pre-designed slip surface. The displacements of the slope surface obtained based on Eq. (1) is indicated in Fig. 7(a), and the time histories of the surface tilting

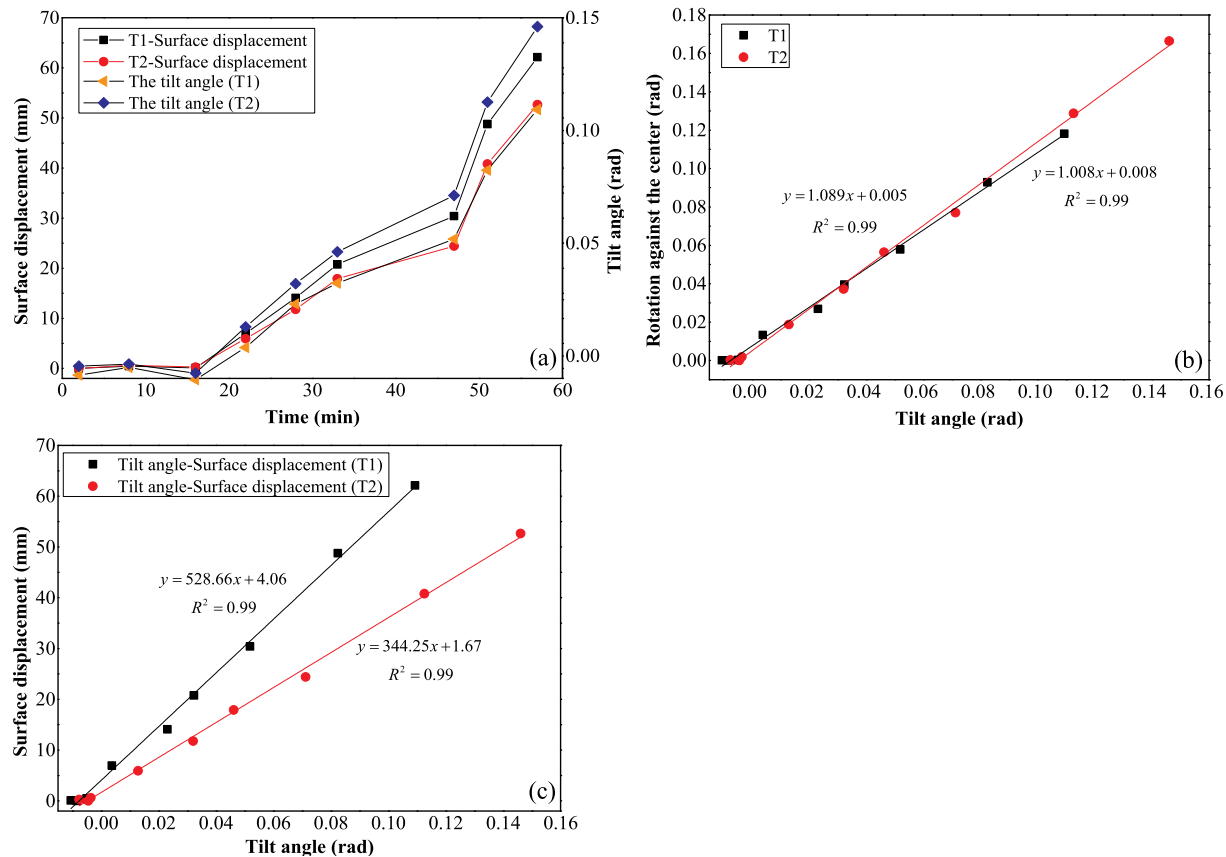


Fig. 10. Results of Test 4. (a) The surface displacements and tilt angles of the slope surface against time, (b) Relationship between the tilt angles of the slope model measured by tilt sensors and the rotational angles of the slope against the centers of the slip surface, (c) Relationship between the surface displacements and tilt angles of the slope surface.

derived from the monitoring data measured by T1, T2 and T3 are also presented in Fig. 7(a). Fig. 7(b) shows the correlation between the surface tilt angles recorded by tilt sensors and the rotational angles of the slope against centers of the slip surface computed using following equation

$$\Delta\theta_i = \arctan \frac{x_{oi} - x_i}{y_{oi} - y_i} - \arctan \frac{x_{oi} - x_i}{y_{oi} - y_i} \quad (2)$$

where $\Delta\theta_i$ is the rotational angles of marked points at slope surface against the centers of the slip surface as shown in Fig. 4. (x_i, y_i) is the position of marked points after sliding, and (x_i, y_i) is the position of the point before slope sliding. (x_{oi}, y_{oi}) is the centers of the slip surface. In this study, if sensors tilt backward, positive tilting angle will be obtained.

The results presented in Fig. 7(b) reveal that the tilt angles coincide with the calculated rotational angles. The relationship between the tilt angle and displacements of the slope surface is presented in Fig. 7(c), in which linear relations are indicated with the coefficients, 1004 mm/rad and 999 mm/rad respectively, approximate to the actual distance between the tilt sensors and the centers of the slip surface as indicated in Fig. A(a).

3.1.2. Results of test 2

Edosaki sand was used in this test, and the radius of the pre-designed slip surface was 600 mm. The dry density of the surface layer

and base layer were 1.25 g/cm³ and 1.70 g/cm³ respectively (Table 1). The slope failure in this test was also induced by rotating the container, and the slope profile as well as the setup of apparatus are presented in Fig. A(b). Fig. 8(a) shows the variation of surface tilt angles and displacements of the slope. Fig. 8(b) presents the relations between the tilt angles measured by tilt sensors and the estimated rotational angle of the slope against centers of the slip surface, which indicates a consistent correlation in these two variables. Fig. 8(c) reveals the relationship between the tilt angles and displacements of the slope surface, and the results as shown in this figure imply that the coefficients of the linear relations of T1, T2 and T3, coinciding well with the real distance between tilt sensors and centers of the slip surface (Fig. A(b)).

3.1.3. Results of test 3

A noncircular slip surface was used in this test, which consisted of two circular parts with different radii as shown in Fig. A(c). The details of test conditions in the test is presented in Table 1. Fig. 9(a) shows the time histories of the surface displacements and tilt angles, while Fig. 9(b) reveals the correlation in surface tilting and the rotation of the slope. The result indicated in Fig. 9(b) shows the consistency with the finding from Test 1 and Test 2. Linear relationships between the tilt angles and slope surface displacements are indicated in Fig. 9(c). The coefficients of these linear relations are 540 mm/rad and 343 mm/rad, and consistent with the actual distance between the tilt sensors and centers of the slip surface as shown in Fig. A(c).

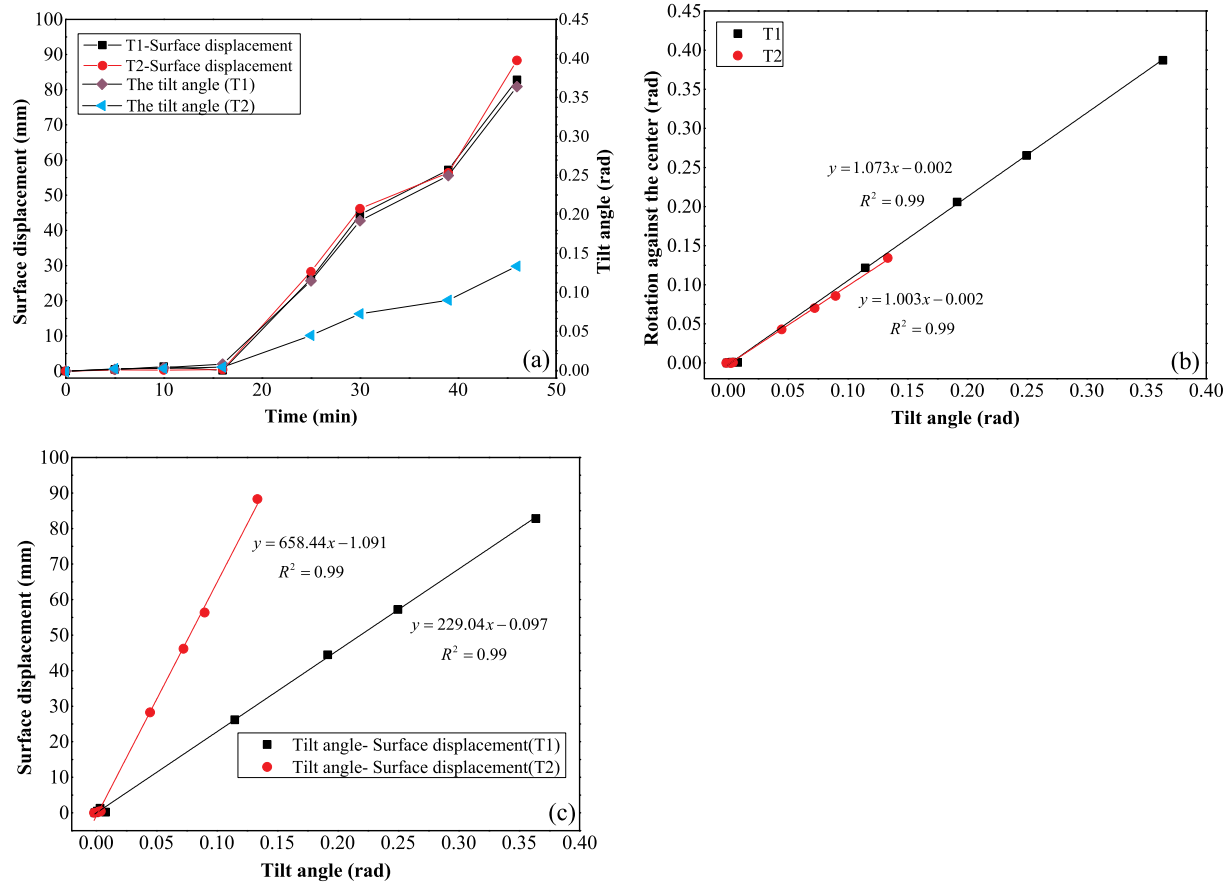


Fig. 11. Results of Test 5. (a) The surface displacements and tilt angles of the slope surface against time, (b) Relationship between the tilt angles of the slope model measured by tilt sensors and the rotational angles of the slope against the centers of the slip surface, (c) Relationship between the surface displacements and tilt angles of the slope surface.

3.1.4. Results of test 4

Test conditions of this test as well as the experimental setup are also indicated in Table and Fig. A(d). Time histories of surface tilting and displacements are presented in Fig. 10(a). Fig. 10(b) shows the relations between the tilt angles recorded by tilt sensors and the rotational angles obtained using Eq. (2). The relationships between the surface tilt angles and displacements are indicated in Fig. 10(c). Fig. 10(b) also imply a consistent correlation in the surface tilting and rotations of the slope, coinciding with the results mentioned before. Similarly, the coefficients of the linear relations as indicated in Fig. 10(c) also approximate to the distance between tilt sensors and the slip surface centers, which was 537 mm and 311 mm (Fig. A(d)).

3.1.5. Results of test 5

In this test, a noncircular slip surface with inconsistent radii was employed as shown in Fig. A(e). The radius of the slip surface was 300 mm in the upper part, and it was 800 mm in the lower part. The slope failure was also triggered by increasing the inclination of the slope, and other details of this test are provided in Table 1 and Fig. A(e). Fig. 11(a) presents the variation in surface tilting angles and displacements, while Fig. 11(b) shows the correlation in surface tilting and the rotations of the slope in which a consistent result is revealed with that

from the tests discussed before. Relationships between the surface tilting and displacements is indicated in Fig. 11(c). Linear relations between these two variables are observed as shown in Fig. 11(c), and the coefficients of the linear relations are also consistent with the distance between the tilt sensors and the centers of the slip surface (Fig. A(e)).

3.1.6. Results of test 6

The slope failure in this test was induced by applying periodical artificial rainfall with a rainfall intensity of 70 mm/h, and the variation in rainfall intensity is presented in Fig. 12(a). Fig. 12(b) shows the time history of tilt angles and displacements of the slope surface, while Fig. 12(c) reveals the correlation in surface tilt angles measured by tilt sensors and the rotational angles of the slope computed using Eq. (2). The results presented in Fig. 12(c) also indicate that a consistent relationship between the tilt angles and rotational angles, and show the consistency with the results from the tests mentioned above. Linear relationships between the tilt angles and displacements of the slope surface are presented in Fig. 12(d), and these results coincide well with that indicated in Test 5 despite that varying triggering factors of slope failure were applied in these two tests. Additionally, the coefficients of the linear relations presented in Fig. 12(d) were 233 mm/rad and

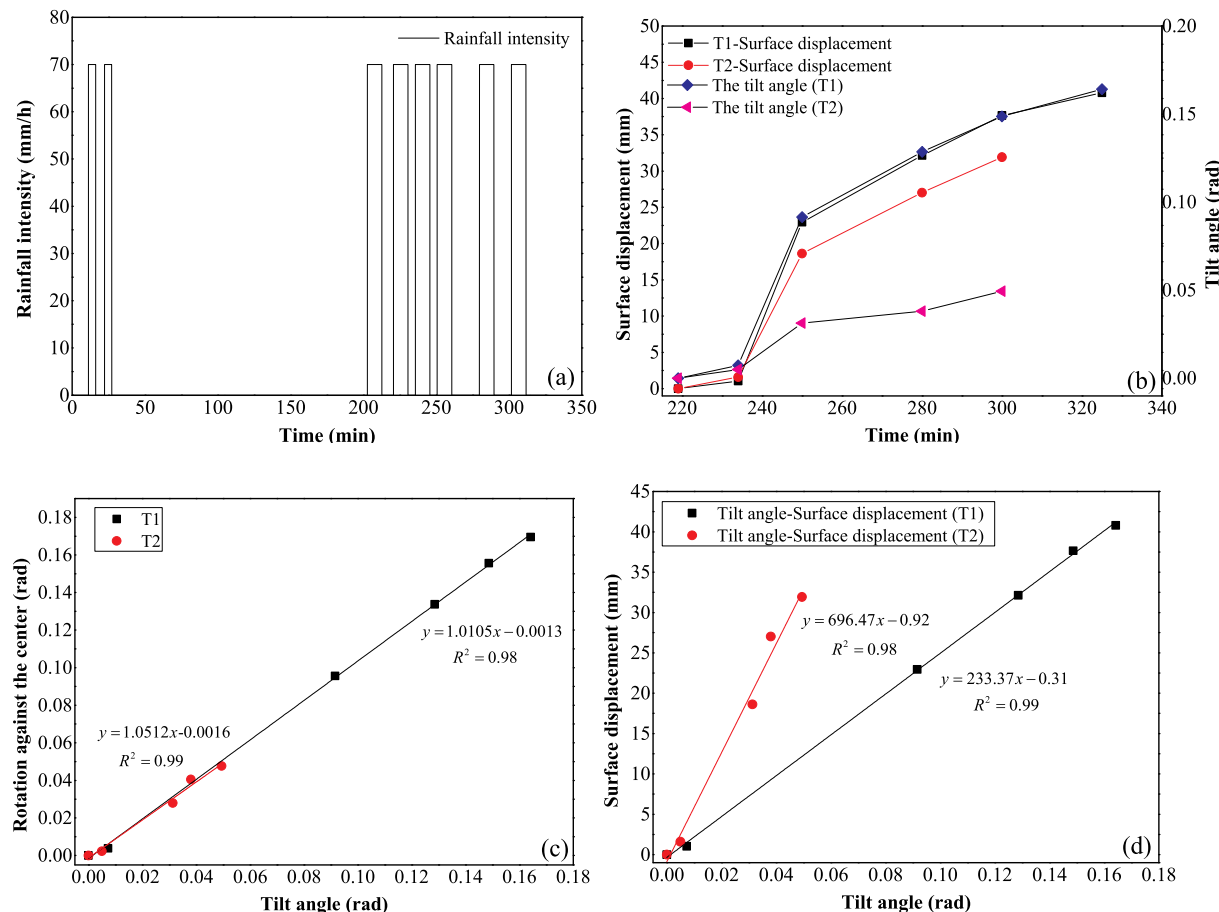


Fig. 12. Results of Test 6. (a) The time history of rainfall intensity, (b) The surface displacements and tilt angles of the slope against time, (c) Relationship between the tilt angles of the slope model measured by tilt sensors and the rotational angles of slopes against the centers of the slip surface, (d) Relationship between the surface displacements and tilt angles of the slope surface.

696 mm/rad, approximating to the actual distance between tilt sensors and the centers of the slip surfaces as indicated in Fig. A(f).

3.1.7. Results of test 7

In this test, the slope failure was triggered by applying continuous rainfall with a rainfall intensity of 70 mm/h. Two tilt sensors (T1 and T2) were employed to measure the tilting behavior of the slope surface, and the surface displacements were recorded by two extensometers (E1 and E2) as shown in Fig. A(g). The time history of surface tilting is presented in Fig. 13(a), while variation in surface displacements are provided in Fig. 13(b). A similar trend was observed in tilt angles and surface displacements as shown in Fig. 13(a) and (b). Fig. 13(c) indicates linear relations between the surface tilt angles and displacement with the coefficients approximating to the actual distance between the tilt sensors and the slip surface centers (Fig. A(g)).

3.2. Results of field test

In the field test, the main slide occurred in the upper part of the slope where tilt sensor T2 and extensometer E2 were installed. The main failure was caused by the rainfall infiltration and crack extension in this region. The surface tilting and displacements of the landslide

mass were recorded by the tilt sensor T2 and extensometer E2, and presented in Fig. 14(a). As shown in Fig. 14(a), the surface tilt angles and displacements increased synchronously at the vicinity of 68 min, and a similar trend in the variation of these two indicators is implied. Fig. 14(b) shows the relation between the tilt angles and displacements of the slope surface, in which a linear relationship is indicated, consistent with the results from laboratory tests.

4. Discussion

4.1. Deformation of active landslides

The deformation of the slope surface is caused by the internal shearing of the landslide masses and the shearing deformation at the slip surface (Rex et al., 1998; Kim, 1999). In previous studies, the surface deformation in active landslides was investigated based on the surface displacement measurements without considering the surface tilting behavior of slopes (Carter and Bentley, 1985a, 1985b; Cruden, 1986; Ulusay and Aksoy, 1994; Intrieri et al., 2012). In this study, detailed investigations on the tilting behavior and displacements of the slope surface were carried out to gain an insight into the sliding mechanism of rotational landslides by performing a series of laboratory

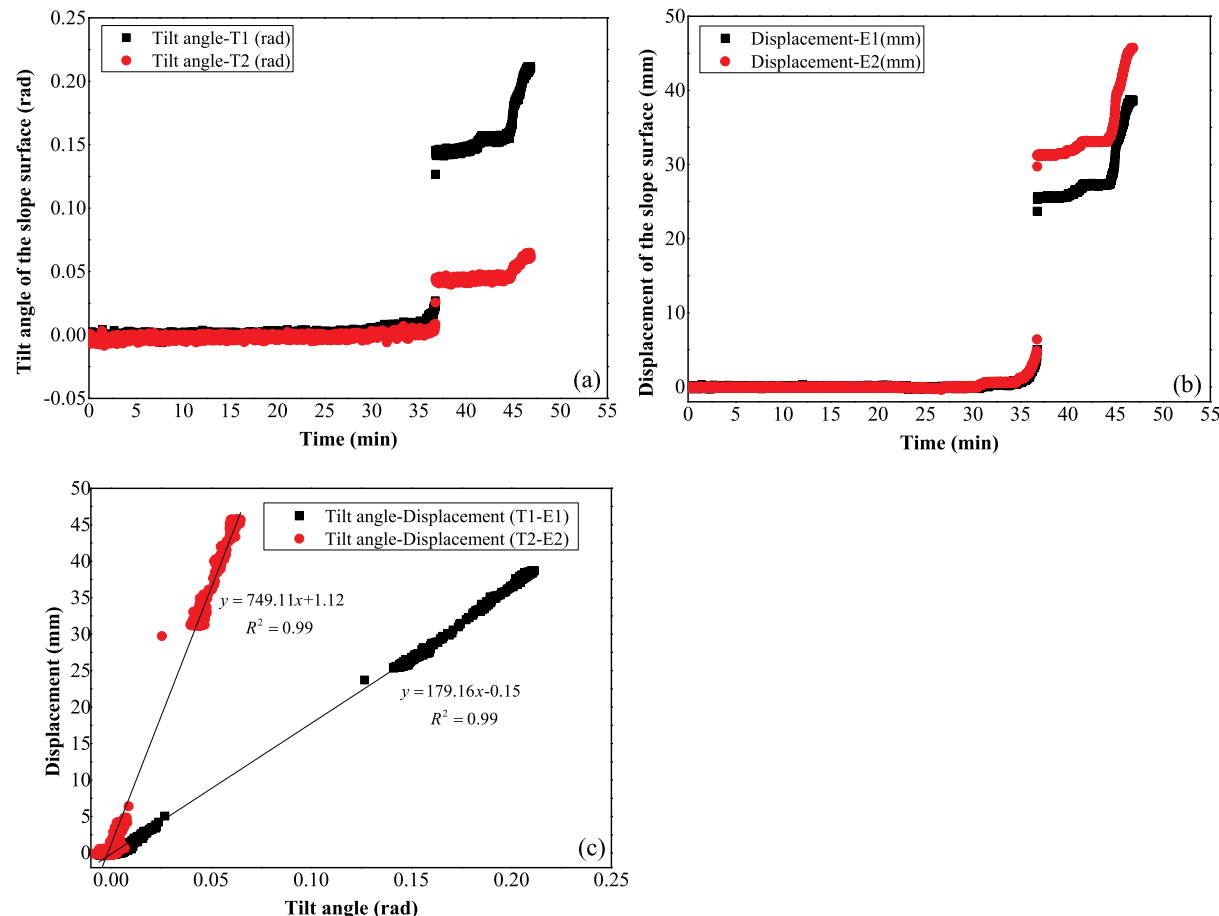


Fig. 13. Results of Test 7. (a) Time history of tilting of the slope surface measured by tilt sensor T1 and T2, (b) Time history of displacements of the slope surface measured by extensometer E1 and E2, (c) Relationship between tilt angles and displacements of the slope surface.

model tests and a field test.

In laboratory model tests, slope models with pre-designed slip surfaces were tested under varying conditions. The results from Test 1 to Test 6 imply that surface tilting recorded by tilt sensors are consistent

with the rotation of the slope surface against centers of the slip surface in spite of the varying experimental conditions in these tests. The consistent correlation indicates that the tilt angles of the slope surface is mainly caused by the rotation of the sliding masses against the centers

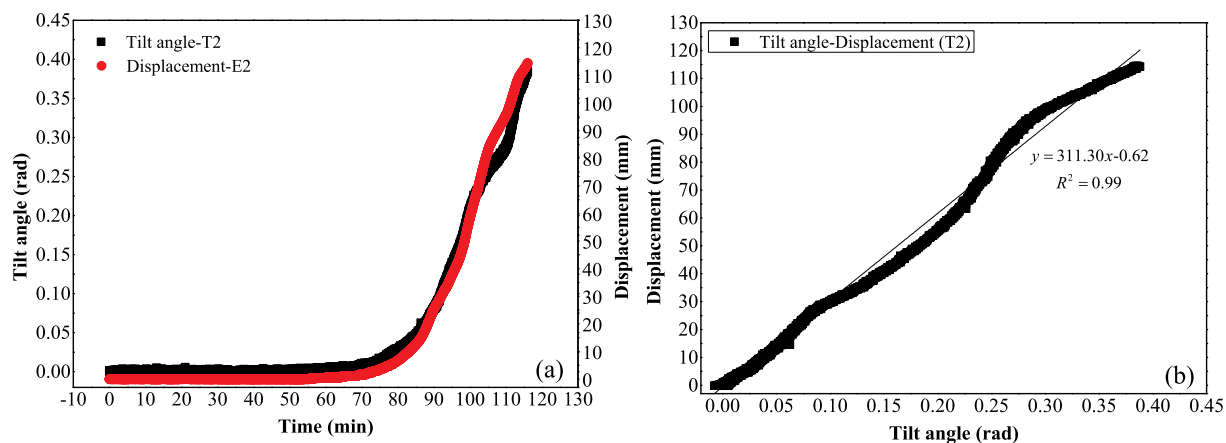


Fig. 14. Results of the field test. (a) Time history of surface tilting and displacements of slopes measured by tilt sensor T2 and extensometer E2 respectively, (b) Relationship between tilt angles and displacements of the slope surface.

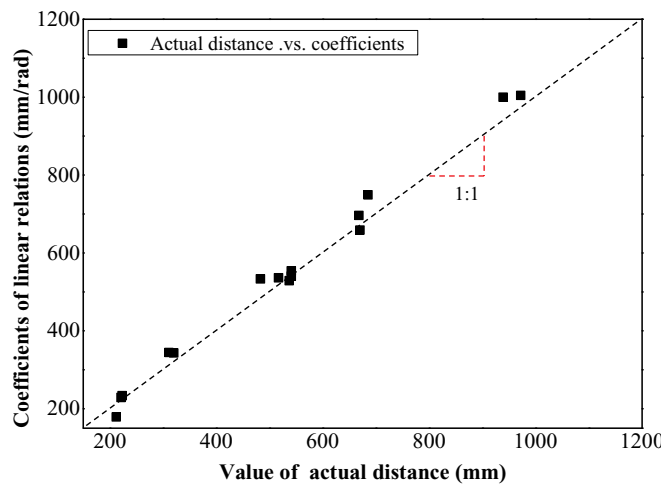


Fig. 15. The value of actual distance between tilt sensors and the centers of the slip surface against the coefficients of the linear relations between the tilt angles and displacements of the slope surface.

of the slip surface or the shearing deformation along the slip surface, while the internal shearing has a negligible influence on the surface tilting based on the results of the laboratory test.

Furthermore, linear relationships between tilt angles and displacements of slope surfaces were also observed in laboratory tests. The coefficients of the linear relations are plotted against the actual distance between the tilt sensors and centers of slip surfaces as shown in Fig. 15, in which a consistent relation with the gradient of 1:1 is revealed. An approximation for the relationship between the surface tilt angles and displacement was proposed based on the results indicated in Fig. 15, which is expressed as

$$\Delta s_i = 2r_i \cdot \tan\left(\frac{\Delta\theta_i}{2}\right) \approx r_i \cdot \Delta\theta_i \quad (3)$$

where Δs_i and $\Delta\theta_i$ are the displacements and tilt angles of the slope surface, respectively. r_i is the actual distance between the tilt sensors installed in the slope and centers of slip surfaces.

The Eq. (3) implies that the deformation at slope surfaces in active rotational landslides with a single slip surface is mainly caused by the sliding or rotation of the landslide masses.

In addition, the results from the field test shows a linear relationship

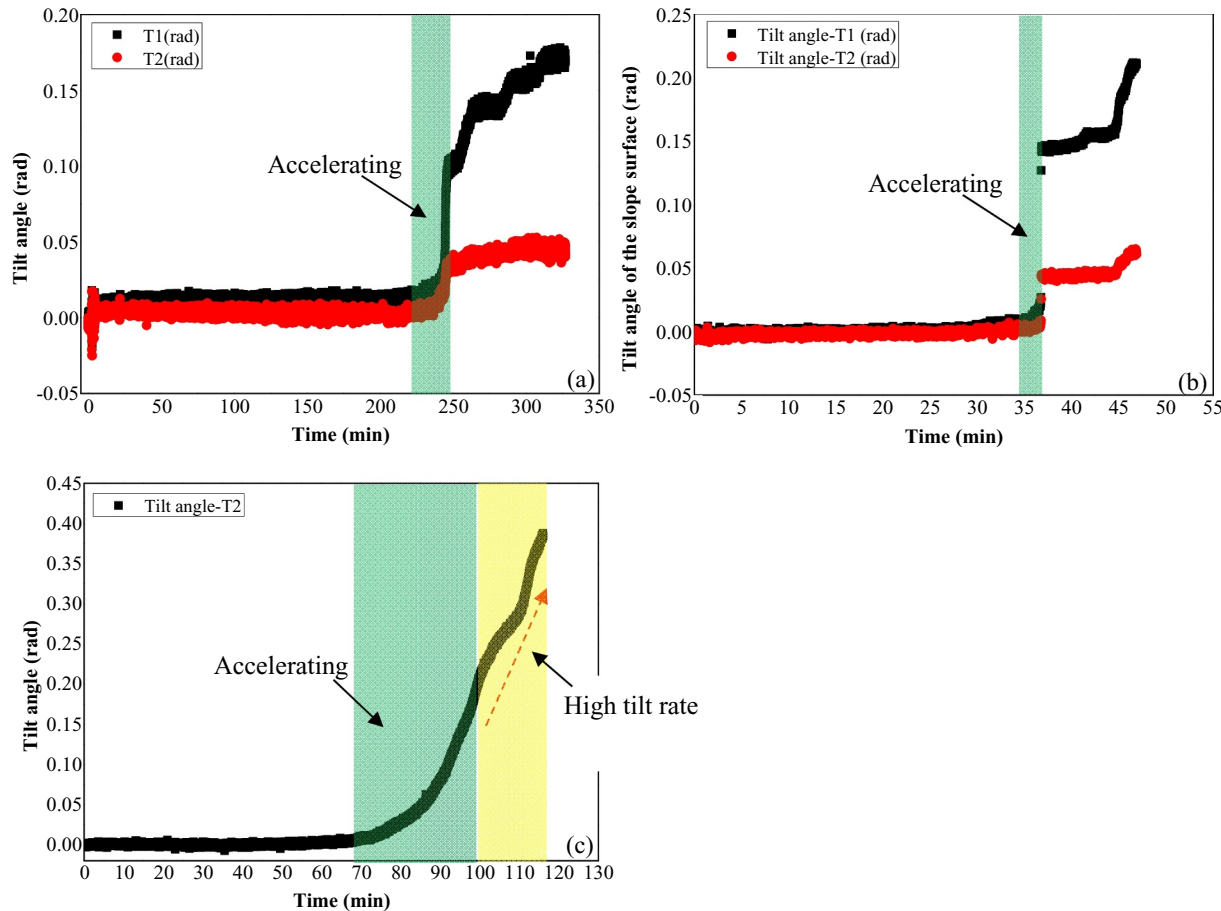


Fig. 16. The time history of tilting of the slope surface for the slope failure induced by applying rainfall. (a) The time history of tilting of the slope surface in Test 6, (b) The time history of tilting of slope surface in Test 7, (c) The time history of tilting of slope surface in the field test.

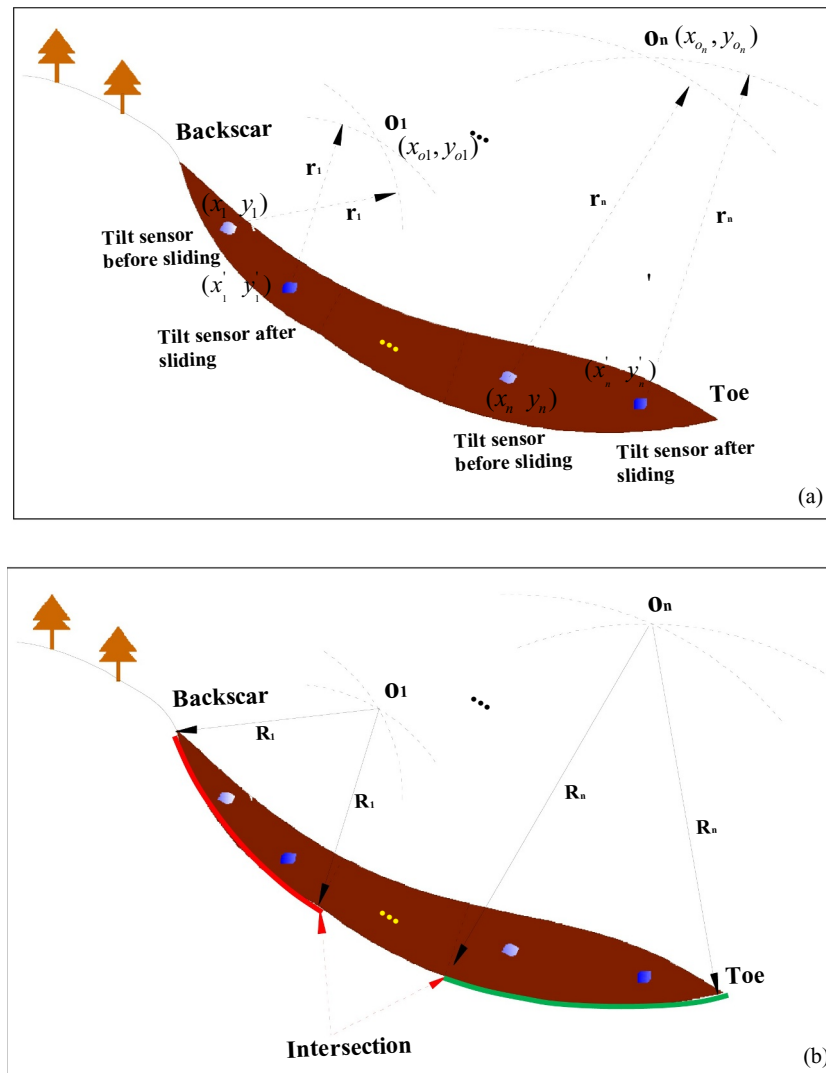


Fig. 17. The method to predict the slip surface: (a) Determine the location of the slip surface center in each part, (b) Predict the segments of the slip surface.

between the tilt angles and displacements of the slope surface as presented in Fig. 14(b). This linear relation implies that the moving mass rotated against a center, and this result provides the field evidence for the Eq. (3).

4.2. Pre-failure tilting behavior in rainfall-induced rotational landslides

The surface tilting was tentatively considered as an implication for the prediction of landslides with rotational components (Voight, 1989; Iverson et al., 2000). In this study, the tilting behavior in rotational landslides induced by rainfall was investigated.

The time histories of surface tilting in Test 6, Test 7 and the field test are presented in Fig. 16. In these tests, the slope failure was triggered by applying rainfall. As shown in Fig. 16(a) and Fig. 16(b), an accelerating stage of tilting was observed before the first failure. It is also noteworthy that an accelerating stage of tilting in the field test was also observed before the slope sliding with a high tilt rate as indicated in

Fig. 16(c). These results imply that the surface tilting measurement of slopes is an effective method to forecast the development of the rotational landslides induced by rainfall.

4.3. Predicting the location of the slip surface in active rotational landslides

Longstanding effort has been made to prediction the slip surface of slopes, and some methods were proposed in recent decades which were based on surface displacements and morphology (Carter and Bentley, 1985a, 1985b; Ulusay and Aksøy, 1994; Rex et al., 1998; Jaboyedoff et al., 2020). The computational process of those methods is complicated and involves many assumptions (Jaboyedoff et al., 2020).

In this paper, a comprehensive investigation on sliding mechanism of rotational landslides was carried out. The test results reveal that the surface deformation of landslide masses is mainly caused by the slope rotation against the centers of slip surfaces when the slope was sliding, and the path of sliding masses is parallel to the slip surfaces. The centers

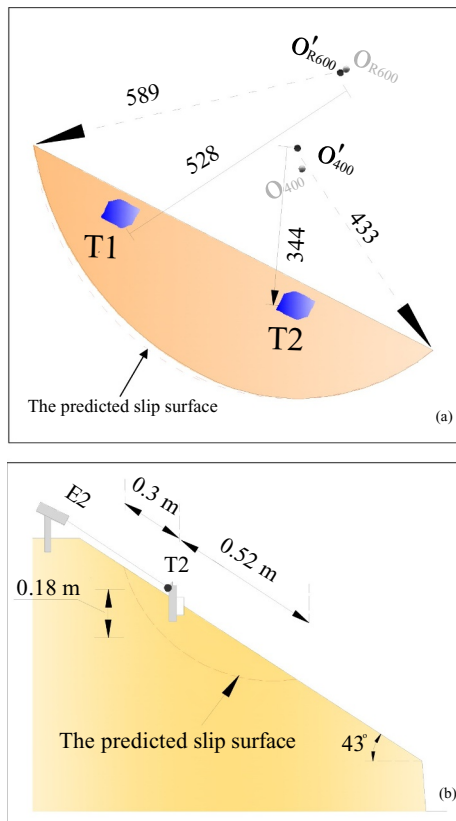


Fig. 18. The case studies for the prediction of the slip surface. (a) The slip surface prediction for Test 4, (b) The slip surface prediction for the field test.

of the slip surfaces in rotational landslides can be achieved based on following equation

$$\begin{cases} (x_{oi} - x_i)^2 + (y_{oi} - y_i)^2 = \left(\frac{\Delta s_i}{\Delta \theta_i}\right)^2 \\ (x_{oi} - x'_i)^2 + (y_{oi} - y'_i)^2 = \left(\frac{\Delta s_i}{\Delta \theta_i}\right)^2 \end{cases} \quad (4)$$

where (x_{oi}, y_{oi}) is the slip surface center of segment i , while (x_i, y_i) is the position of the tilt sensor installed in segment i before the slope sliding, and (x'_i, y'_i) is the position of the tilt sensor in this segment after the slope sliding. Δs_i is the surface displacements of segment i , and $\Delta \theta_i$ is the tilt angles of segment i measured by the tilt sensor. r_i is the radius of the slip surface of segment i . The definition of parameters in Eq. (4) is illustrated in Fig. 17.

The process for the prediction of the slip surface is as follows (Fig. 17):

1. Divide the slide mass into several segments by bisecting the zone between two successive tilt sensors.
2. Estimate the centers of the slip surface of each segment using Eq. (4) as shown Fig. 17(a).
3. Construct the slip surface of each segment from edges of the slope to middle parts by drawing an arc of the circle defined by the slip

surface centers and endpoints (scar, toe or the intersections) of each block derived from step 1 and step 2 (Fig. 17(b))

Two case studies were carried out to validate the proposed method for estimating the depth of slip surfaces, and the results are presented in Fig. 18. Fig. 18(a) shows the predicted slip surface of the slope model in Test 4, in which noncircular slip surface was used. The reconstructed slip surface shows a slight difference with the pre-designed slip surface as indicated in the figure, and the centers of the estimated slip surfaces (O_{R600} and O_{R400}) are approximate to the pre-designed ones (O_{600} and O_{400}) as presented in Fig. 18(a). Fig. 18(b) shows the predicted slip surface in the field test, and the radius of the estimated slip surface is around 50 cm. Although the position of the real slip surface in the field test was difficult to be identified accurately, the depth of the predicted slip surface at the position where tilt sensor T2 was installed, is 18 cm, consistent with the real depth of the slip surface measured by a scale during the test.

With the development of new technologies, such as InSAR, laser scanner, photogrammetry, and so on, the surface deformation of slopes is increasingly easier to be obtained. The study provided detailed investigations on mechanism of rotational landslides based on the slope surface tilting measurements, and will enable the estimation of the development of a rotational landslide using the data obtained by the remote sensing technologies.

5. Conclusions

In this paper, investigations on the tilting behavior and displacements of slope surfaces were carried out by performing a series of the laboratory tests and a field test. The results of this study revealed that the monitoring of slope surface tilting provides useful information for the reconstruction of slip surfaces of rotational landslides and for the prediction of their sliding behavior. The major findings of this study are presented as follows,

1. A linear relationship between the tilt angles and displacements of the slope surface was documented through laboratory and field tests, and a specific equation that describes the relation was also proposed.
2. The deformation of slope surface in an active rotational landslide is mainly attributed to the sliding or rotation of the landslide masses along the slip surface.
3. The pre-failure tilting behavior in rotational landslides induced by rainfall can be forecasted using surface tilting measurements.
4. A simplified method to reconstruct the slip surface was proposed, and validated by the tests in this study.

Declaration of Competing Interest

None.

Acknowledgements

This research was supported by Chinese Scholarship Council (CSC, Grant No.201506370052) for PhD studies of the first author, and the Grants-in-Aid for Scientific Research of the Japan Society for the Promotion of Science (JSPS), Core-to-Core Program B (No. 16H04407).

Appendix

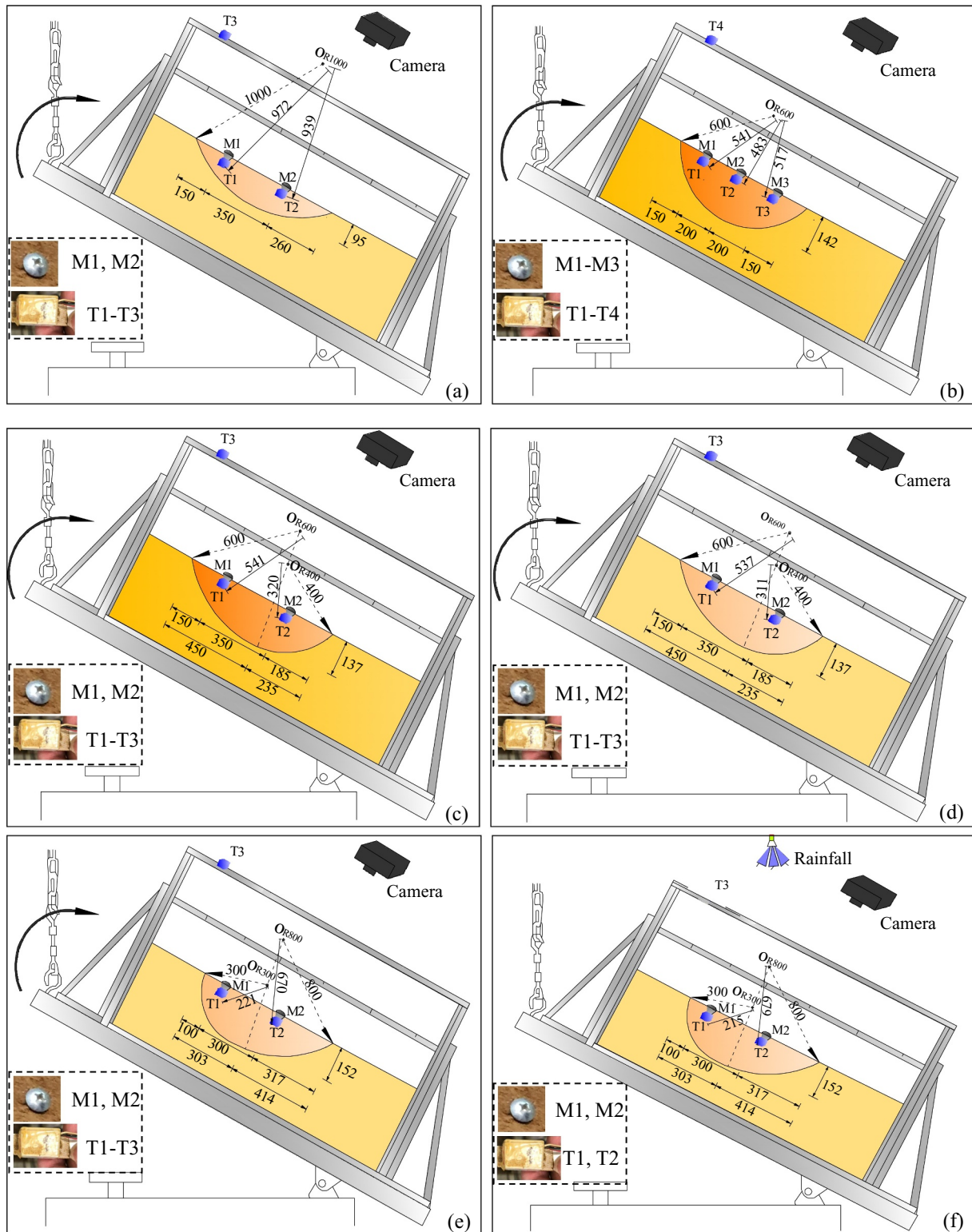
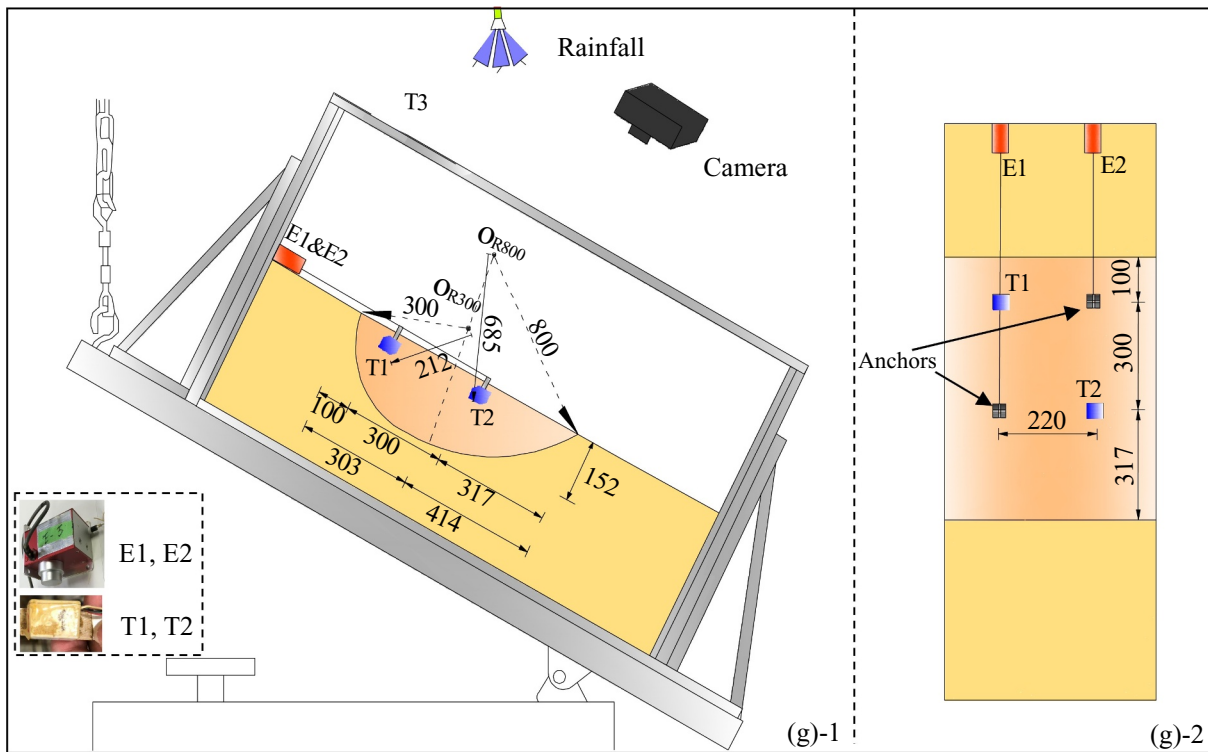


Fig. A. The illustration of laboratory model tests. (a) The illustration of the arrangement of apparatuses and the cross section of the slope model in Test 1, (b) The illustration of the arrangement of apparatuses and the cross section of the slope model in Test 2, (c) The illustration of the arrangement of apparatuses and the cross section of the slope model in Test 3, (d) The illustration of the arrangement of apparatuses and the cross section of the slope model in Test 4, (e) The illustration of the arrangement of apparatuses and the cross section of the slope model in Test 5, (f) The illustration of the arrangement of apparatuses and the cross section of the slope model in Test 6, (g) The illustration of the arrangement of apparatuses and the cross section of the slope model in Test 7.



References

- Abhirup, D., Satyam, D.N., Towhata, I., 2018. Early warning system using tilt sensors in Chibo, Kalimpong, Darjeeling Himalayas, India. *Nat. Hazards* 94, 727–741.
- Carlà, T., Farina, P., Intrieri, E., Ketizmen, H., Casagli, N., 2018. Integration of ground-based radar and satellite InSAR data for the analysis of an unexpected slope failure in an open-pit mine. *Eng. Geol.* 235, 39–52.
- Carter, M., Bentley, S.P., 1985a. The geometry of slip surfaces beneath landslides: predictions from surface measurements. *Can. Geotech. J.* 22, 234–238.
- Carter, M., Bentley, S.P., 1985b. A procedure to locate slip surfaces beneath active landslides using surface monitoring data. *Comput. Geotech.* 1, 139–153.
- Crosta, G.B., Agliardi, F., 2003. Failure forecast for large rock slides by surface displacement measurements. *Can. Geotech. J.* 40, 176–191.
- Cruden, D.M., 1986. The geometry of slip surfaces beneath landslides: predictions from surface measurements:¹ Discussion. *Can. Geotech. J.* 23, 94.
- Dixon, N., Simth, A., Flint, J.A., Khanna, R., Clark, B., Andjelkovic, M., 2018. An acoustic emission landslide early warning system for communities in low-income and middle-income countries. *Landslides* 15, 1631–1644.
- Fukuzono, T., 1985. A new method for predicting the failure time of slopes. In: Proceedings of the 4th International Conference & Field Workshop on Landslides, Tokyo, pp. 145–150.
- Intrieri, E., Gigli, G., Mugnai, F., Fanti, R., Casagli, N., 2012. Design and implementation of a landslide early warning system. *Eng. Geol.* 147, 124–136.
- Intrieri, E., Raspini, F., Fumagalli, A., Lu, P., Del Conte, S., Farina, P., Allievi, J., Ferretti, A., Casagli, N., 2017. The Maoxian landslide as seen from space: detecting precursors of failure with Sentinel-1 data. *Landslides* 15, 123–133.
- Iverson, R.M., Reid, M.E., Iverson, N.R., LaHusen, R.G.L.M., Mann, J.E., Brien, D.I., 2000. Acute Sensitivity of Landslide rates to initial Soil Porosity. *Science* 290, 513–516.
- Jaboyedoff, M., Demers, D., Locat, J., Locat, A., Locat, P., Oppikofer, T., Robitaille, D., Turnet, D., 2009. Use of terrestrial laser scanning for the characterization of retrogressive landslides in sensitive clay and rotational landslides in river banks. *Can. Geotech. J.* 46, 1379–1390.
- Jaboyedoff, M., Dario, C., Marc-Henri, D., Thierry, O., Marin, P., Benjamin, R., 2020. A review of methods used to estimate initial landslide failure surface depths and volumes. *Eng. Geol.* <https://doi.org/10.1016/j.enggeo.2020.105478>.
- Kim, M.B., 1999. Determination of translational landslide slip surface depth using balanced cross sections. *Environ. Eng. Geosci.* 5 (2), 147–156.
- Kuroki, K., Ishikawa, K., Nishikawa, J., 1995. Forecast time and analysis of rupture mechanism using video-tape records for a rock failure of out slope. In: Proceedings of the 8th ISRM Congress, Tokyo, pp. 399–402.
- Ochiai, H., Okada, Y., Furuya, G., Okura, Y., Matsui, T., Sammori, T., Terajima, T., Sassa, K., 2004. A fluidized landslide on a natural slope by artificial rainfall. *Landslides* 1, 211–219.
- Petley, D.N., Bulmer, M.H., Murphy, W., 2002. Patterns of movement in rotational and translational landslides. *Geology* 30 (8), 719–722.
- Rex, L.B., James, M., Robert, W.F., 1998. Surface deformation as a guide to kinematics and three-dimensional shape of slow-moving, clay-rich landslides, Honolulu, Hawaii. *Environ. Eng. Geosci.* 4 (3), 283–306.
- Saito, M., 1969. Forecasting time of slope failure by tertiary creep. In: Proceedings, 7th international conference on soil mechanics and foundation engineering, Mexico City, pp. 677–683.
- Smethurst, J.A., Smith, A., Uhlemann, S., Wooff, C., Chambers, J., Hughes, P., Lenart, S., Springman, S.M., Lofroth, H., Hughes, D., 2017. Current and future role of instrumentation and monitoring in the performance of transport infrastructure slopes. *Q. J. Eng. Geol. Hydrogeol.* 50, 271–286.
- Sornette, D., Helmstetter, A., Andersen, J.V., Gluzman, S., Grasso, J.-R., Pisarenko, V., 2004. Towards landslide predictions: two case studies. *Phys. A* 338, 605–632.
- Stähli, M., Sättle, M., Huggel, C., McDowell, B.W., Lehmann, P., Van, H.A., Berne, A., Schleiss, M., Ferrari, A., Kos, A., Or, D., Springman, S.M., 2015. Monitoring and prediction in early warning systems for rapid mass movements. *Nat. Hazards Earth Syst. Sci.* 15 (4), 905–917.
- Teuku, F.F., Dwikorita, K., Wahyu, W., 2016. An integrated methodology to develop a standard for landslide early warning systems. *Nat. Hazards Earth Syst. Sci.* 16, 2123–2135.
- Towhata, I., Uchimura, T., Gallage, C.P.K., 2005. On early detection and warning against rainfall-induced landslide. In: Proc. of The First General Assembly and The Fourth Session of Board of Representatives of the International Consortium on Landslides (ICL). Springer, Washington, DC, pp. 133–139.
- Uchimura, T., Towhata, I., Trinh, T.L.A., Fukuda, J., Carlos, J.B.B., Wang, L., Seko, I., Uchida, T., Matsuoka, A., Ito, Y., Onda, Y., Iwagami, S., Kim, M.S., Sakai, N., 2010. Simple monitoring method for precaution of landslides watching tilting and water contents on slopes surface. *Landslides* 7, 351–357.
- Uchimura, T., Towhata, I., Lin, W., Nishie, S., Yamaguchi, H., Seko, I., Jiangping, Q., 2015. Precaution and early warning of surface failure of slopes by using tilt sensors. *Soils Found.* 55 (5), 1086–1099.
- Uhlemann, S., Smith, A., Chambers, J., Dixon, N., Meldrum, P., Dijkstra, T., Haslam, E., Merritt, A., Gunn, D., 2016. Assessment of ground-based monitoring techniques applied to landslide investigations. *Geomorphology* 253 (1), 438–451.
- Ulusay, R., Aksoy, H., 1994. Assessment of the failure mechanism of a highwall slope under spoil pile loadings at a coal mine. *Eng. Geol.* 38, 117–134.
- Voight, B., 1988. A method for prediction of volcanic eruptions. *Nature* 332, 125–130.
- Voight, B., 1989. A relation to describe rate-dependent material failure. *Science* 243, 200–203.
- Wang, G.H., Sassa, K., 2003. Pore-pressure generation and movement of rainfall-induced landslides: effects of grain size and fine-particle content. *Eng. Geol.* 69, 109–125.
- Wasowski, J., Bovenga, F., 2014. Investigating landslides and unstable slopes with satellite multitemporal interferometry: current issues and future perspectives. *Eng.*

- Geol. 174, 103–138.
- Wasowski, J., Bovenga, F., 2015. Remote sensing of landslide motion with emphasis on satellite multitemporal interferometry applications: An overview. In: Shroder, J.F., Davies, T. (Eds.), Landslide hazards, risks and disasters. Elsevier Inc, Amsterdam, pp. 345–403. <https://doi.org/10.1016/B978-0-12-396452-6.00011-2>.
- Wasowski, J., Pisano, L., 2019. Long-term InSAR, borehole inclinometer, and rainfall records provide insight into the mechanism and activity patterns of an extremely slow urbanized landslide. *Landslides*. <https://doi.org/10.1007/s10346-019-01276-7>. (Published online).
- Xie, J.R., Uchimura, T., Wang, G.H., Shen, Q., Maqsood, Z., Xie, C.R., Lei, W.K., Tao, S., Chen, P., Dong, H., Mei, G.X., Qiao, S.F., 2019. A new prediction method for the occurrence of landslides based on the time history of tilting of the slope surface. *Landslides*. 17, 301–312.